Characterization of silver species on graphitic carbon nitride nanosheets as promoters for photocatalytic carbon dioxide reduction under visible light with a mononuclear ruthenium(II) complex

Journal:	Journal of Materials Chemistry A
Manuscript ID	TA-ART-04-2018-003245.R1
Article Type:	Paper
Date Submitted by the Author:	23-Apr-2018
Complete List of Authors:	Maeda, Kazuhiko ; Tokyo Institute of Technology, Chemistry An, Daehyeon; Tokyo Institute of Technology, Chemitry Ranasinghe, Chandana Sampath; Toyota Kogyo Daigaku, Uchiyama , Tomoki ; Kyoto University, Graduate School of Human and Environmental Studies Kuriki, Ryo; Tokyo Institute of Technology, Department of Chemistry Kanazawa, Tomoki; Tokyo Institute of Techlogy Lu, Daling; Tokyo Institute of Technology, Center for Advanced Materials Analysis Nozawa, Shunsuke; High Energy Accelerator Research Organization, Photon Factory Yamakata, Akira; Toyota Technological Institute, Graduate School of Enginnering Uchimoto, Yoshiharu; Kyoto University, Department of Energy & Hydrocarbon Chemistry, Graduate School of Engineering Ishitani, Osamu; Tokyo Institute of Technology, Department of Chemistry

ARTICLE

Characterization of silver species on graphitic carbon nitride nanosheets as promoters for photocatalytic carbon dioxide reduction under visible light with a mononuclear ruthenium(II) complex†

Kazuhiko Maeda,*[a] Daehyeon An,[a] Chandana Sampath Kumara Ranasinghe,[b] Tomoki Uchiyama,[c] Ryo Kuriki,[a,d] Tomoki Kanazawa,[a] Daling Lu,[e] Shunsuke Nozawa,[f] Akira Yamakata,[b] Yoshiharu Uchimoto,[c] Osamu Ishitani[a]

Hybrid photocatalysts constructed with a mononuclear Ru(II)-complex (**RuP**), silver nanoparticles, and carbon nitride nanosheet (NS-C_3N_4) photocatalyze CO_2 reduction to selectively form formate under visible light. The structure of the nanoparticulate silver species, which worked as promoters for the reaction, was characterized by X-ray diffraction, UV-VIS diffuse reflectance spectroscopy, high-resolution transmission microscopy, and X-ray absorption fine-structure spectroscopy. The silver promoters were loaded on the surface of NS-C_3N_4 by an impregnation method from an aqueous solution containing $AgNO_3$ or an in-situ photodeposition method. Impregnation of NS-C_3N_4 with 2.0 wt% Ag followed by reduction with H_2 at 473 K (further modified with **RuP**) resulted in the highest photocatalytic activity, giving a turnover number of 5700 (based on **RuP**), which was the greatest value among the formate-generating hybrid systems with a mononuclear complex. While the optimized photocatalyst contained highly dispersed Ag_2O-like nanoclusters as the major silver species, experimental results suggested that highly dispersed Ag^0 species are more important for enhancing CO_2 reduction activity. That is; the obtained experimental results led us to conclude that there are two major factors affecting activity: one is the feature size of silver species (smaller is better), and the other is oxidation state of silver (metallic is better).

Introduction

CO_2 reduction on a heterogeneous photocatalyst has been extensively studied as a means of chemical fixation of CO_2, an inert molecule that causes green house effect.[1–4] So far, several types of photocatalysts have been reported, including nanoparticle-loaded semiconductors,[5–13] and metal-complex/semiconductor hybrids.[14–27]

In metal oxide photocatalysts, it has been reported that silver species deposited on the metal oxide surface promote photocatalytic CO_2 reduction.[6,7,9–13] Because Ag^0 is a good

a. Department of Chemistry, School of Science, Tokyo Institute of Technology, 2-12-1-NE-2 Ookayama, Meguro-ku, Tokyo 152-8550, Japan. E-mail: maedak@chem.titech.ac.jp
b. Graduate School of Engineering, Toyota Technical Institute, 2-12-1 Hisakata, Tempaku, Nagoya 468-8511, Japan
c. Graduate School of Human and Environmental Studies, Kyoto University, Nihonmatsu-cho, Yoshida, Sakyo-ku, Kyoto 606-8317, Japan.
d. Japan Society for the Promotion of Science, Kojimachi Business Center Building, 5-3-1, Kojimachi, Chiyoda-ku, Tokyo 102-0083, Japan.
e. Suzukakedai Materials Analysis Division, Technical Department, Tokyo Institute of Technology 4259 Nagatsuta-cho, Midori-ku, Yokohama 226-8503, Japan
f. Institute of Materials Structure Science, High Energy Accelerator Research Organization, 1-1 Oho, Tsukuba, Ibaraki 305-0801, Japan
† Electronic Supplementary Information (ESI) available: [additional XRD data]. See DOI: 10.1039/x0xx00000x

electrocatalyst for CO_2 reduction,[28] Kudo et al. first applied nanoparticulate Ag^0 as a cocatalysts for CO_2 reduction on $ALa_4Ti_4O_{15}$ (A = Ca, Sr, and Ba) layered perovskites having 3.79–3.85 eV band gaps. The Ag^0-loaded materials showed photocatalytic activity for CO_2 reduction to form CO and water oxidation into O_2 under UV irradiation ($\lambda > 200$ nm), although H_2 evolution, which is an undesirable side reaction during CO_2 reduction, occurred simultaneously. Following this work, several groups reported similar systems consisting of a wide-gap oxide semiconductor and silver nanoparticles. Some of them exhibited very high selectivity to CO_2 reduction, while suppressing proton reduction to release H_2.[7,11,12] These studies claimed that Ag^0 nanoparticles on semiconductors work as active sites (i.e., cocatalysts) for catalytic CO_2 reduction,

Because these metal-oxide photocatalysts only work under UV irradiation due to their large band gaps, it is highly desirable to develop a visible-light-responsive photocatalytic system from the viewpoint of solar energy conversion. Our group has been developing such visible-light-active photocatalysts, with a focus on hybrids that consist of a narrow-gap non-oxide semiconductor (such as oxynitrides and nitrides) and a functional metal complex.[15,16,19,21,23] For example, carbon nitride (C_3N_4) modified with a mononuclear Ru(II) complex,[15,19,20] binuclear Ru(II)-Ru(II) complex,[22] or

Ru(II)-Re(I) complex[24] showed photocatalytic activity for CO_2 reduction into formate or CO under visible light ($\lambda > 400$ nm). Carbon source of the product in these systems was confirmed by isotope tracer experiments with $^{13}CO_2$ to be CO_2. Importantly, the photocatalytic performance both in the mononuclear- and the binuclear systems using C_3N_4 to yield formate was significantly improved by modification with Ag nanoparticles.[22] Transient absorption spectroscopy indicated that nanoparticulate silver species on C_3N_4 collected electrons, which were likely to move to the loaded Ru complex, thereby promoting photocatalytic CO_2 reduction.[22] Interestingly, however, silver species loaded on visible-light-responsive (oxy)nitride semiconductors did not efficiently serve as a cocatalyst for CO_2 reduction without Ru complexes,[16,22] clearly different from those loaded on metal oxide photocatalysts. In any of photocatalytic systems, it is important to understand the structure–activity relationship toward the construction of more efficient systems. At present, however, local structure of the loaded silver species in metal-complex/semiconductor hybrids as well as its impact on photocatalytic performance for CO_2 reduction has not been investigated in detail. Consequently, no guideline to improve the photocatalytic activity with respect to structure of silver species is available.

In the present study, we investigated the structure of silver-modified carbon nitride nanosheets (NS-C_3N_4) by means of X-ray diffraction (XRD), UV-VIS diffuse reflectance spectroscopy (DRS), transmission electron microcopy (TEM), and X-ray absorption spectroscopy (XAFS). In addition, transient absorption (TA) spectroscopy, which is a powerful technique that can visualize photogenerated carrier dynamics in a semiconductor material,[29–31] was conducted in order to investigate the impact of the loaded Ag species on the behavior of photogenerated charge carriers in NS-C_3N_4. Relationship between structural characteristics of silver-modified NS-C_3N_4 and photocatalytic activity for CO_2 reduction with the aid of a mononuclear Ru(II) complex (**RuP**) is discussed. An illustration of the present CO_2 photoreduction system is shown in Scheme 1. Through the optimization of the Ag loading conditions, we not only elucidated the optimal structure of the loaded Ag species, but also realized highly stable and selective CO_2-to-formate conversion with a record turnover number of 5700 in mononuclear metal complex/semiconductor hybrid photocatalysts.
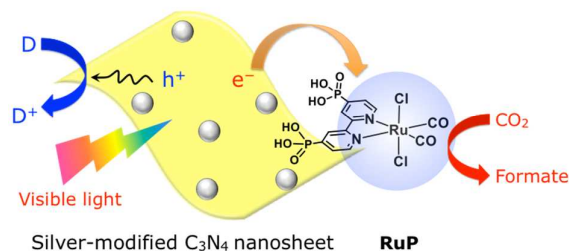
Scheme 1. Photocatalytic CO_2 reduction on **RuP**-adsorbed, silver-modified NS-C_3N_4 under visible light.

Experimental

Synthesis of carbon nitride nanosheets

Carbon nitride nanosheets used in this work were synthesized as follows. First, 10 g of urea (99+%, Wako Chemicals Co.) was heated in air at a ramp rate of 2.3 K min^{-1} to 873 K, keeping that temperature for 4 h, then cooling without temperature control. The as-prepared carbon nitride was activated by thermal H_2 treatment.[32] 100 mg of the sample was heated in a H_2 stream (20 mL min^{-1}) at a ramp rate of 10 K min^{-1} to 773 K, keeping that temperature for 1 h, then cooling naturally. For simplicity, the as-prepared material is represented hereafter as NS-C_3N_4. The specific surface area determined by nitrogen adsorption experiment at 77 K was 63 m^2 g^{-1}.

Modification of NS-C_3N_4 with silver species

Silver species as promoters were loaded onto the surface of NS-C_3N_4 by an impregnation method using $AgNO_3$ (>99.8%, Wako Pure Chemicals Co.) as the precursor. 50 mg of NS-C_3N_4 was dispersed in an aqueous $AgNO_3$ solution (10 mL). The water content was subsequently removed under reduced pressure at 317 K. The resulting solid sample was heated under a H_2 stream (20 mL min^{-1}) or static air at 373–623 K for 1 h in the same manner as described above. The amount of Ag loading ranged from 0 to 5.0 wt%.

Ag loading was also done by a photodeposition method. 100 mg of NS-C_3N_4 was dispersed in an aqueous $AgNO_3$ solution (100 mL) containing 10 vol% methanol (>99.8%, Kanto Chemicals Co.), followed by degassing and irradiation with a 300 W xenon lamp ($\lambda > 300$ nm) for 2 h to reduce Ag^+ ions to Ag^0. After collecting the resulting solid by filtration, the as-prepared Ag-loaded NS-C_3N_4 was dried under reduced pressure overnight.

Adsorption of RuP onto silver-modified NS-C_3N_4

RuP was synthesized according to the method reported in our previous paper.[19] The successful synthesis of **RuP** was confirmed by ^{1}H nuclear magnetic resonance (NMR) and Fourier transform infrared (FT-IR) spectroscopy and by elemental analysis.

Adsorption of **RuP** onto NS-C_3N_4 was conducted as follows. 40 mg of the silver-modified C_3N_4 was dispersed in an acetonitrile (MeCN) solution (20 mL) of **RuP**. The suspension was stirred at room temperature in dark overnight to allow for adsorption/desorption equilibrium, followed by filtration and washing with acetonitrile. The filtrates were collected and concentrated to a volume of 30 mL. The amount of **RuP** absorbed was calculated based on the UV-vis spectrum of the filtrate, using the equation:

Adsorbed amount (mol g^{-1})

$$= \frac{A_{\text{before}} - A_{\text{after}}}{A_{\text{before}}}$$

$$\cdot \frac{C \text{ (mol L}^{-1}) \times 20 \times 10^{-3}\text{(L)}}{40 \times 10^{-3}\text{(g)}}$$

where A_{before} and A_{after} are the absorbance of the solution before and after the adsorption procedure, respectively, and C is the initial concentration of the complex.

Characterization of Materials

The prepared materials were characterized by X-ray diffraction (XRD) (MiniFlex600, Rigaku; Cu Kα radiation), UV–VIS–NIR diffuse reflectance spectroscopy (DRS) (V-565, Jasco), and transmission electron microscopy (TEM) (JEM-2010F, JEOL). The Brunauer–Emmett–Teller (BET) surface area of each specimen was determined using a BELSOEP-mini instrument (BEL Japan) at liquid nitrogen temperature. The amount of carbon, nitrogen and oxygen were determined by elemental analysis (MICRO CORDER JM10, J-SCIENCE) by Suzukakedai Materials Analysis Division, Technical Department, Tokyo Institute of Technology.

XAFS measurements of Ag–K edge spectra were carried out at the AR-NW10A beamline of the PF-AR (High Energy Accelerator Research Organization, Tsukuba, Japan) under the approval of the Photon Factory Advisory Committee (Proposal No. 2014S2-006) and the BL01B1 beamline of the SPring-8 synchrotron facility (Hyogo, Japan) using a ring energy of 8 GeV and a stored current of 100 mA in the top-up mode (Proposal No. 2017B1040 and 2017B1438). XAFS spectra were acquired at room temperature in the fluorescence or transmittance mode using a Si(311) double-crystal-monochromator. The data for XAFS spectra were processed using the Athena.[33] The Fourier transforms of k^3-weighted EXAFS spectra were typically in the 3.0–12.0 Å region.

Time-resolved IR Absorption Measurements

Measurements were obtained using a home-made spectrometer described previously.[29,30] Powders of NS-C$_3$N$_4$ and silver-modified NS-C$_3$N$_4$ were loaded on a CaF$_2$ plate at a density of 1.5 mg cm^{-2} and placed into an IR cell for measurements. The samples were photoexcited using a 355 nm UV pulse from an Nd:YAG laser (Continuum Surelite I, duration: 6 ns, power: 0.3 mJ, repetition rate: 5–0.1 Hz), and transient absorptions in visible to mid-IR region were measured in vacuum. The time resolution of this spectrometer was limited to 1–2 μs by the bandwidth of the amplifier (Stanford Research Systems, SR560, 1 MHz).

Photocatalytic reactions

Reactions were performed at room temperature (298 K) using an 8 mL test tube containing 4 mL of a mixed solution of *N,N*-dimethylacetamide (DMA) and triethanolamine (TEOA) (4:1 v/v) and 4 mg of the photocatalyst powder. Prior to irradiation, the suspension was purged with CO$_2$ (Taiyo Nippon Sanso Co., >99.995%) for 20–30 min. A 400 W high pressure Hg lamp (SEN) was used as a light source, in combination with a NaNO$_2$ solution as a filter to provide visible light irradiation (λ > 400 nm). The gaseous reaction products were analyzed using a gas chromatograph with a thermal conductivity detector (GL Science, Model GC323). The formate generated in the liquid phase was analyzed via a capillary electrophoresis system (Otsuka Electronics Co., Model CAPI-3300).

Apparent quantum yield for the formate generation was measured using a 300 W xenon lamp (Asahi Spectra Co., MAX-303) and a band-pass filter (λ = 400 nm) with the light intensity of 7.3 mW in the same manner as reported previously.[19,22] In this case, 20 mg of **RuP**(27.9 μmol g^{-1})/Ag(2.0 wt%)/NS-C$_3$N$_4$ powder was employed for the reaction.

Purification of organic solvents

Organic solvent used in this work was subject to purification prior to use. DMA was dried over molecular sieves 4A (which was heated at 373 K under reduced pressure (< 1 Torr) overnight for several days), and distilled under reduced pressure (10–20 Torr). Methanol was used after distillation. MeCN was distilled over P$_2$O$_5$ twice, and then distilled over CaH$_2$ prior to use. TEOA was distilled under reduced pressure (<1 Torr). The distilled DMA and TEOA were kept under Ar prior to use.
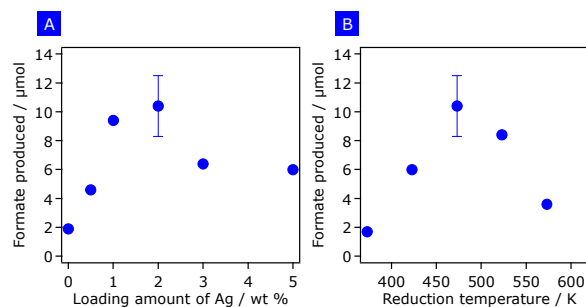

Fig. 1. Dependence of formate generation over Ag-modified NS-C$_3$N$_4$ on (A) the loading amount of Ag with a common heating temperature of 473 K and (B) the heating temperature with a common loading amount of 2.0 wt% Ag. Reaction conditions: catalyst, 4.0 mg; reactant solution, a mixed solution of DMA and TEOA (4:1 v/v, 4.0 mL); light source, 400 W high-pressure Hg lamp with a NaNO$_2$ aqueous solution filter. Reaction time: 5 h.

Results and discussion

Photocatalytic activity

First we tested silver-modified NS-C$_3$N$_4$ prepared by an impregnation, H$_2$-reduction method as the component of **RuP**/Ag/NS-C$_3$N$_4$ hybrid photocatalyst. Note here that the preparation conditions of Ag/NS-C$_3$N$_4$ did not influence the adsorption of **RuP**; in all cases, nearly quantitative adsorption (1.9–2.0 μmol g^{-1}) was achieved, and that **RuP** does not have absorption in visible light region.[19]

Fig. 1A shows the dependence of formate generation on the loading amount of Ag using samples treated at a common heating temperature of 473 K. Here the activity was improved abruptly with an increase in the loading amount of Ag up to 2.0 wt%, beyond which it began to drop. The activity was also found to depend strongly on the heating temperature, as shown in Fig. 1B. Formate generation was increased almost linearly as the temperature rose up to 473 K, then decreasing monotonically. In all cases, selectivity to formate was 85–95% (except for unloaded one), with some byproduction of H$_2$. We also investigated possible formation of other products such as formaldehyde and methane. However, no additional product

other than formate and H_2 was observed, except for a trace amount of CO, which was undetectable in most cases.

At the optimal condition, an apparent quantum yield of 4.2% (at 400 nm) and a catalytic turnover number (TON) of 5775 (with respect to the mole amount of **RuP**, which is the active site for CO_2 reduction) were obtained (Fig. 2), indicative of catalytic cycle of the reaction. Importantly, the high selectivity to formate generation (>90%) was kept even after extended period of the reaction, meaning that **RuP** on the optimized Ag/NS-C_3N_4 worked very efficiently. Here it is also noted that the obtained TON value is obviously higher than the previously reported values (1000–1400),[19,22] and is the highest one among the formate-generating hybrids constructed with a mononuclear metal complex and a semiconductor. Reproducibility tests using different batch of samples showed that there was an error of 20% in formate generation at the optimal condition. Without **RuP**, Ag-modified NS-C_3N_4 (2.0 wt%, 423 K) produced a small amount of H_2, not formate. This again confirmed that Ag species on NS-C_3N_4 did not effectively work as cocatalysts for CO_2 reduction, and that **RuP** was indispensable for the reaction to proceed. As discussed in our previous paper,[19] we think that hydrogen bondings are formed between –NH_2 groups on NS-C_3N_4 and –PO_3H_2 groups derived from **RuP**. However, we could not elucidate the exact location of **RuP** on Ag/NS-C_3N_4 at present. Considering the fact that the CO_2 reduction reaction was significantly promoted by Ag loading on NS-C_3N_4, it is likely that the relative location of **RuP** and Ag nanoparticles is close enough to afford electron transfer between the two.
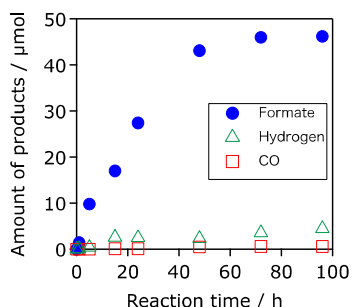

Fig. 2. A typical time course of CO_2 reduction on the optimized **RuP**/Ag/NS-C_3N_4 under visible light. Reaction conditions: catalyst, 4.0 mg; reactant solution, a mixed solution of DMA and TEOA (4:1 v/v, 4.0 mL); light source, 400 W high-pressure Hg lamp with a $NaNO_2$ aqueous solution filter.
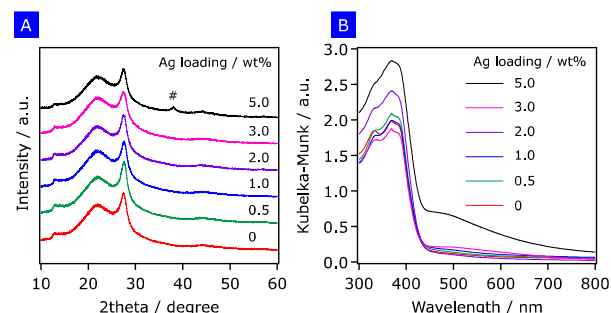

Fig. 3. (A) XRD patterns and (B) UV-VIS diffuse reflectance spectra of NS-C_3N_4 modified with different amounts of Ag at a common temperature of 473 K. The # mark in the panel (A) is assigned to (111) diffraction peak of Ag^0. A broad peak at around 22 degree in XRD patterns originated from a glass folder for the measurement.
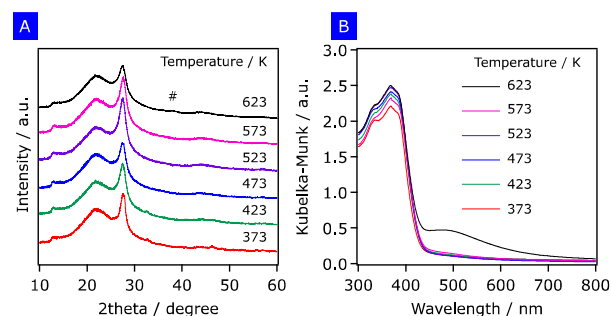

Fig. 4. (A) XRD patterns and (B) UV-VIS diffuse reflectance spectra of 2.0 wt% Ag-modified NS-C_3N_4 treated at different temperatures. The # mark in the panel (A) is assigned to (111) diffraction peak of Ag^0. A broad peak at around 22 degree in XRD patterns originated from a glass folder for the measurement. An enlarged view of the XRD pattern of the 623 K sample is shown in Fig. S1.

Structural characterization

To investigate the relationship between photocatalyst structure and activity for photocatalytic CO_2 reduction using Ag-modified NS-C_3N_4, the synthesized materials were characterized by XRD, UV–visible DRS, HR-TEM and XAFS. As shown in Fig. 3A, XRD analyses for Ag-modified NS-C_3N_4 having different Ag amounts showed no sign of silver species up to 3.0 wt%. At 5.0 wt%, however, a small peak assigned to Ag^0 was observed. Fig. 3B shows DRS of the same set of samples. Spectral feature is similar to each other at lower Ag content, but the background in longer wavelength regions tends to be more pronounced at higher loadings. This absorption can be assignable to Ag^0. Similar tendencies were observed in samples treated at different temperatures with a common Ag amount (Fig. 4). That is, with increasing temperature, absorption feature assignable to Ag^0 was observed in DRS.
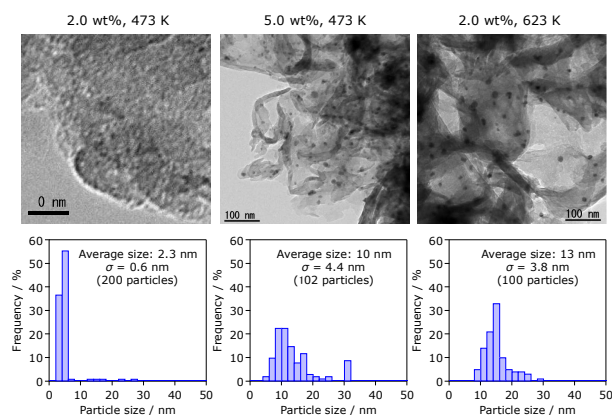

Fig. 5. (Top) TEM images and (bottom) the corresponding Ag-particle size distributions of Ag-loaded NS-C_3N_4 treated with H_2 under different conditions.

The generation of larger Ag^0 species was confirmed by TEM observations. Here, the loaded silver species could be distinguishable because of the difference in electron density between silver and NS-C_3N_4. As shown in Fig. 5, samples

prepared with larger Ag loadings or treated at higher temperatures contained larger silver species with an average size of 10–13 nm. On the other hand, silver species in the 2.0 wt% sample (heated at 473 K) were highly dispersed in the form of nanoparticles having an average size of 3.6 nm without noticeable aggregation.

Because neither XRD nor DRS gave us sufficient information on the structure of silver species in samples prepared at lower Ag loadings or temperatures, the local structure of silver was investigated by means of XAFS, which is a powerful technique to identify nanoparticulate cocatalysts on a semiconductor photocatalyst.[9,10,34–38] Regarding analysis of surface-deposited nanoparticles, it is well known that X-ray photoelectron spectroscopy (XPS) is another representative technique. In the case of silver species, however, XPS gives small shifts in binding energy for Ag^+ state compared with the metallic Ag^0 state.[39,40] Kaushik also suggested X-ray excited Auger spectroscopy as an alternative means to investigate oxidation state of silver species.[40] Although we measured Auger spectra for the prepared silver-modified samples, no peak was detected unfortunately most likely due to its low concentration of the silver species.

Fig. 6A shows Ag K-edge EXAFS spectra of the same set of samples. It is first noted that the oscillation profiles of the samples clearly differ from that of $AgNO_3$ reference, indicating that the impregnated $AgNO_3$ species are decomposed upon the subsequent heat treatment with H_2 at 473 K. The oscillation profiles of Ag-modified NS-C_3N_4 with smaller Ag loadings at smaller k regions are similar to that of the Ag_2O reference, but not perfectly the same. The EXAFS oscillation tended to be clearer with an increase in the Ag loading. Importantly, contribution from Ag^0 was more pronounced with increasing the loading amount, while reducing the extent of the oscillation derived from Ag_2O. This tendency is more obvious in the FT of EXAFS spectra, as displayed in Fig. 6B.
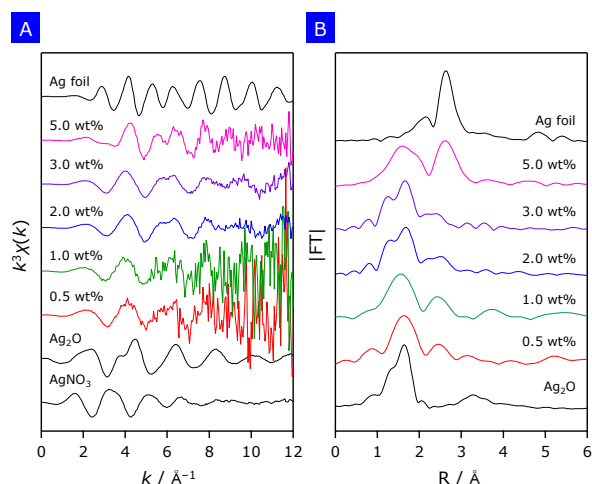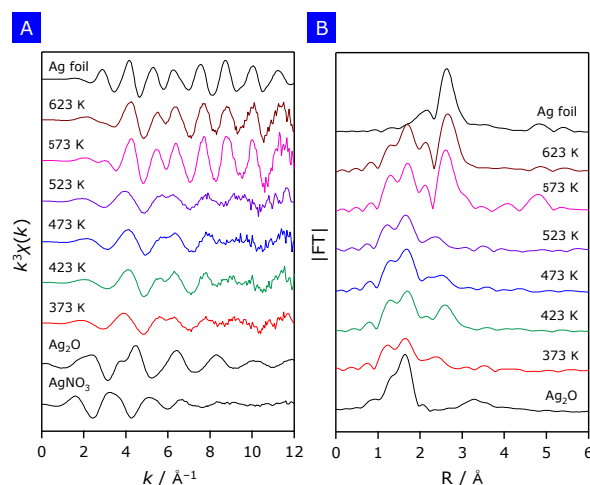

Fig. 7. (A) Ag K-edge EXAFS spectra and (B) FT of EXAFS spectra for 2.0 wt% Ag-modified NS-C_3N_4 treated at different temperatures.

EXAFS spectra for samples treated at different reduction temperatures with a common Ag loading amount of 2.0 wt% are shown in Fig. 7. Even at 373 K heating, the spectral feature was different from the $AgNO_3$ precursor, but similar to Ag_2O with some mixing of Ag^0. With increasing the heating temperature, the contribution derived from Ag^0 was more distinct, as can be seen both in the EXAFS oscillation profiles and FT of EXAFS spectra. This is reasonable, because increasing heating temperature with H_2 should result in more reduction of cationic Ag species. Even at the highest temperature of 623 K, however, some contributions from Ag_2O remained. The results of EXAFS analyses for samples with higher Ag loadings or higher heating temperatures are consistent with the results of XRD and DRS (Figs 3 and 4).

It was thus shown that Ag species loaded on NS-C_3N_4 are close to Ag_2O at lower loadings and temperatures, but Ag^0 co-existed with some aggregations at higher loadings and temperatures to some extent. Result of elemental analysis indicated that the as-synthesized NS-C_3N_4 contained ca. 5.0 wt% oxygen, which is large enough to be the source of the Ag_2O-like species even at 5.0 wt% Ag loading. Therefore, the remaining oxygen species in NS-C_3N_4 might be the source of "Ag_2O" observed in XAFS measurements. It should be noted that other oxynitride-type semiconductors (such as Y-Ta oxynitride) modified with Ag in the same impregnation, H_2-reduction method contained Ag^0 dominantly.[41] Thus, the formation of "Ag_2O-like species" observed in this study appears to originate from strong interaction between the loaded silver species and the NS-C_3N_4 surface.

Factors affecting activity

The results of photocatalytic reaction and structural characterization indicate that the photocatalytic activity of **RuP**/Ag/NS-C_3N_4 for CO_2 reduction is dependent on the physicochemical state of silver deposits on NS-C_3N_4. More concretely, it appears that Ag_2O-like nanoparticles having higher dispersion on NS-C_3N_4 contributed to the enhanced

Fig. 6. (A) Ag K-edge EXAFS spectra and (B) FT of EXAFS spectra for NS-C_3N_4 modified with different amounts of Ag at a common reduction temperature of 473 K.

activity, while aggregation and/or excess coverage of silver species had a negative impact on activity. For example, the activity was decreased from 2.0 to 3.0 wt% despite the fact that these two samples contained almost the same Ag_2O-like structure (Fig. 6). Such an excess loading of silver species on the $NS-C_3N_4$ surface could hinder active sites for redox reactions; in this case, most likely oxidation reaction, thereby lowering the overall efficiency. At present, however, we could not judge whether or not Ag^0 had a promotional effect on activity, because samples prepared with larger Ag loadings or treated at higher temperatures (i.e., less active samples) contained both Ag_2O and Ag^0.

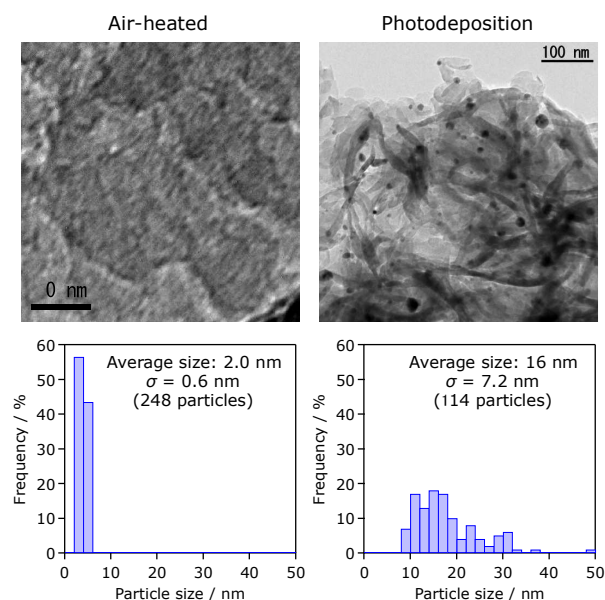**Fig. 8.** (Top) TEM images and (bottom) the corresponding Ag-particle size distributions of 2.0 wt% Ag-loaded $NS-C_3N_4$ prepared by an impregnation method with air-heating and a photodeposition method.

To investigate the possible impact of Ag^0 on activity, additional two samples were prepared as follows. One was prepared by a similar impregnation method using $AgNO_3$ as the precursor (2.0 wt% Ag content), but followed by air heating at 473 K, in which the formation of Ag^0 may be minimized. The other one was synthesized by an in-situ photodeposition method, where Ag^0 is supposed to be dominantly deposited.

Compared to the optimized sample prepared at 2.0 wt% Ag

with 473 K H_2 reduction, the air-treated sample showed no significant change in XRD and DRS (Fig. S2). TEM observations indicated that the air-treated sample contained highly dispersed silver species having an average size of 2.0 nm, similar to the optimized H_2-reduced sample (Fig. 8). By contrast, the photodeposition sample showed a clear sign of Ag^0 formation (Fig. S2), with relatively large size (17 nm in average). EXAFS analyses for these samples showed that the air-treated sample dominantly contained Ag_2O-like structure that is similar to the optimal H_2-reduced sample, while Ag^0 was the major species in the photodeposition sample (Fig. 9).

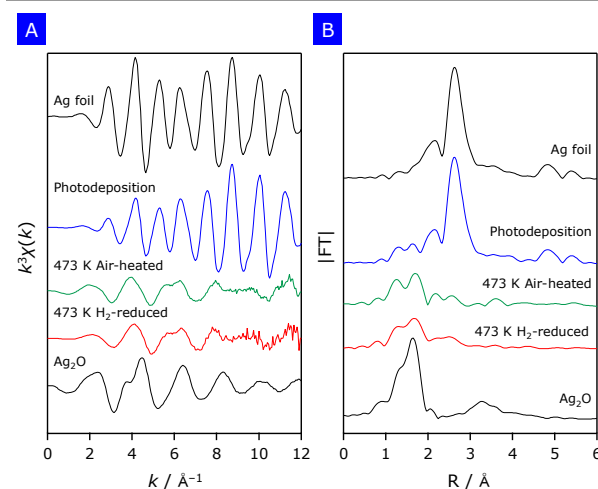**Fig. 9.** (A) Ag K-edge EXAFS spectra and (B) FT of EXAFS spectra for 2.0 wt% Ag-modified $NS-C_3N_4$ treated in air and prepared by an in-situ photodeposition method. The data for the optimized sample (2.0 wt% Ag with 473 K H_2-reduced) is also shown.

Using the as-prepared two additional samples, visible-light CO_2 reduction was conducted with the aid of **RuP** in the same manner. The results are listed in Table 1. Interestingly, the activity of the air-treated sample was lower than that of H_2-reduced one, even though it had almost the same local structure of Ag_2O with identical size, as judged from TEM observation and EXAFS measurement (Figs. 8 and 9). The photodeposition sample also exhibited lower activity than the best-performing one did. However, the photodeposition sample, even which contained larger Ag^0 size with wider distribution, worked much better than the sample prepared at 623 K H_2 that contained both Ag^0 and Ag_2O with smaller sizes and narrower distribution. This result indicates that Ag^0 had better promotional effect than Ag_2O-like species, although we

Table 1. Photocatalytic activities of 2.0 wt% Ag-loaded $NS-C_3N_4$, further modified with **RuP**, for CO_2 reduction under visible light ($\lambda > 400$ nm)[a]

Entry	Sample	Contained silver species[b]	Average size of the deposited silver species[c] / nm	Formate produced / μmol	Selectivity to formate / %
1	Unloaded	-	-	1.9	73
2	H_2-reduced at 473 K	Ag_2O	3.6	10.4±2.1	95
3	Air-treated at 473 K	Ag_2O	2.0	7.0±0.8	92
4	Photodeposition	Ag^0	17	6.5	94
5	H_2-reduced at 623 K	$Ag^0 + Ag_2O$	13	2.3±0.3	83

[a] Reaction conditions: catalyst, 4.0 mg; reactant solution, a mixed solution of DMA and TEOA (4:1 v/v, 4.0 mL); light source, 400 W high-pressure Hg lamp with a $NaNO_2$ aqueous solution filter. Reaction time: 5 h. [b] Determined by XAFS. [c] Based on TEM observations.

could not realize highly dispersed Ag^0 nanoparticles on NS-C$_3$N$_4$ due to a technical difficulty at this moment. Nevertheless, further increase in activity should be possible if one can modify NS-C$_3$N$_4$ with highly dispersed Ag^0. The fact that the H$_2$-reduced sample was better than the air-treated one may support the idea, as silver species in the former is closer to Ag^0 than that in the latter (although there is little difference in EXAFS spectra between the two samples).
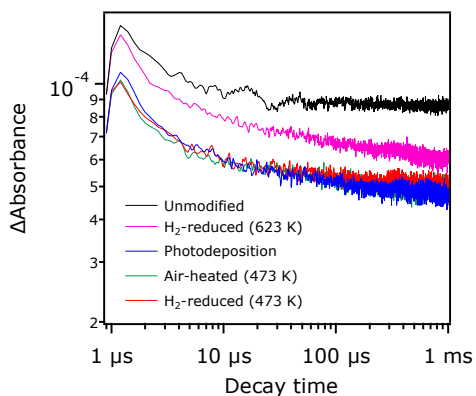

Fig. 10. Decay curves of transient absorption intensity at 1800 cm^{-1} for silver-modified NS-C$_3$N$_4$ samples. Excitation: 355 nm (under vacuum).

We also conducted TA spectroscopy in order to investigate how the behavior of photogenerated charge carriers of NS-C$_3$N$_4$ changes with respect to the loading conditions of silver. Fig. 10 shows time courses of transient absorption intensity of the five samples (listed in Table 1) at 1800 cm^{-1}, which results from shallowly trapped and/or free electrons generated in a semiconductor material.[31] Compared to unmodified NS-C$_3$N$_4$, all of the silver-modified samples exhibited more pronounced decays, indicating that the photogenerated electrons in NS-C$_3$N$_4$ are able to move to the loaded silver species. This observation is consistent with that in our previous work using Ag-loaded mesoporous g-C$_3$N$_4$.[22] Durrant et al. reported that transient absorption signals in the visible and NIR regions, derived from photogenerated electrons, were decreased upon loading of Pt on carbon nitride.[42] The electron-accepting nature of the loaded metal is consistent with our present study using silver species. Although some early reports claimed that Ag$_2$O on C$_3$N$_4$ works exclusively as a hole collector,[43–45] the present study clearly demonstrated that Ag$_2$O-like species serves as an electron trap similar to Ag^0.

However, we stress here that there is no correlation between the decay behavior of each sample and the activity, although the relatively slow decay of the sample reduced at 623 K with H$_2$ may account for the lowest activity among the tested materials (see Table 1). At present, we could not evaluate how electrons accumulated in the deposited silver species on NS-C$_3$N$_4$ transfer to **RuP**, because of technical difficulties. Therefore, electron transfer efficiency from the loaded species to **RuP** may differ with respect to the physicochemical state of the loaded silver species, thereby

affecting the activity of the **RuP**/Ag/NS-C$_3$N$_4$ system. This is currently under investigation in our laboratory.

Conclusions

Nanoparticulate silver species are effective promoters for visible-light CO$_2$ reduction on a hybrid photocatalyst constructed with a mononuclear Ru(II) complex (**RuP**) and C$_3$N$_4$. By varying preparation conditions of silver loading on C$_3$N$_4$ nanosheets, the highest activity was obtained with a sample prepared by an impregnation, H$_2$-reduction method at 473 K and 2.0 wt% Ag loading. The optimal photocatalyst gave the highest turnover number of formate generation (5700) among the mononuclear complex/semiconductor hybrids ever reported, while keeping the high selectivity (>90%) even for extended period of reaction (96 h). EXAFS analyses and TEM observations revealed that the optimized photocatalyst contained highly dispersed Ag$_2$O-like nanoparticles as the major silver species. Experimental results also indicated that Ag^0 was more suitable as the promoter than Ag$_2$O, if each particle size is similar. The results of this work thus suggested that the formation of highly dispersed Ag^0 nanoparticles on C$_3$N$_4$ will be the key to achieve highly efficient visible-light CO$_2$ reduction with **RuP**, although it still remains a challenge.

Conflicts of interest
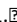
There are no conflicts to declare.

Acknowledgements

Author contributions

K.M. designed the project and wrote a draft of the manuscript. D.A. conducted most of the experiments and analyses with R.K. C.S.K.R. and A.Y performed transient absorption spectroscopy. T.U., T.K., S.Y., and Y.U. performed XAFS measurement with D.A. D.L. conducted TEM observations. R.K. and K.M. designed the **RuP** complex with O.I. All of the authors discussed and provided comments on the experiments and the manuscript during preparation.

Notes and references

1   S. Sato, T. Arai and T. Morikawa, *Inorg. Chem.*, 2015, **54**, 5105.
2   Y. Yamazaki, H. Takeda and O. Ishitani, *J. Photochem. Photobiol. C: Photochem. Rev.,* 2015, **25**, 106.
3   R. Kuriki and K. Maeda, *Phys. Chem. Chem. Phys.,* 2017, **19**, 4938.
4   K. Maeda, *Progress in Solid State Chem.,* 2018, in press. DOI: 10.1016/j.progsolidstchem.2017.11.003.
5   T. Yui, A. Kan, C. Saitoh, K. Koike, T. Ibusuki and O. Ishitani, *ACS Appl. Mater. Interfaces,* 2011, **3**, 2594.
6   K. Iizuka, T. Wato, Y. Miseki, K. Saito and A. Kudo, *J. Am. Chem. Soc.*, 2011, **133**, 20863.
7   K. Teramura, Z. Wang, S. Hosokawa, Y. Sakata and T. Tanaka, *Chem. Eur. J.*, 2014, **20**, 9906.
8   J. Hong, W. Zhang, Y. Wang, T. Zhou and R. Xu, *ChemCatChem,* 2014, **6**, 2315.
9   M. Yamamoto, T. Yoshida, N. Yamamoto, T. Nomoto, Y. Yamamoto, S. Yagi and H. Yoshida, *J. Mater. Chem. A*, 2015, **3**, 16810.
10 M. Yamamoto, T. Yoshida, N. Yamamoto, T. Nomoto, A. Yamamoto, H. Yoshida and S. Yagi, *J. Phys: Conf. Ser.,* 2016, **712**, 012074.
11 R. Pang, K. Teramura, H. Asakura, S. Hosokawa and T. Tanaka, *Appl. Catal. B: Environ.,* 2017, **218**, 770.
12 H. Nakanishi, K. Iizuka, T. Takayama, A. Iwase and A. Kudo, *ChemSusChem,* 2017, **10**, 112.
13 A. Anzai, N. Fukuo, A. Yamamoto and H. Yoshida, *Catal. Commun.,* 2017, **100**, 134.
14 S. Sato, T. Morikawa, S. Saeki, T. Kajino and T. Motohiro, *Angew. Chem., Int. Ed.*, 2010, **49**, 5101−5105.
15 K. Maeda, K. Sekizawa and O. Ishitani, *Chem. Commun.,* 2013, **49**, 10127.
16 K. Sekizawa, K. Maeda, K. Koike, K. Domen and O. Ishitani, *J. Am. Chem. Soc.,* 2013, **135**, 4596.
17 J. Lin, Z. Pan and X. Wang, *ACS Sustainable Chem. Eng.*, 2014, **2**, 353.
18 S. Wang, J. Lin and X. Wang, *Phys. Chem. Chem. Phys.,* 2014, **16**, 14656.
19 R. Kuriki, K. Sekizawa, O. Ishitani and K. Maeda, *Angew. Chem., Int. Ed.,* 2015, **54**, 2406.
20 C. D. Windle, E. Pastor, A. Reynal, A. C. Whitwood, Y. Vaynzof, J. R. Durrant, R. N. Perutz and E. Reisner, *Chem. Eur. J.*, 2015, **21**, 3746.
21 R. Kuriki, O. Ishitani and K. Maeda, *ACS Appl. Mater. Interfaces,* 2016, **8**, 6011.
22 R. Kuriki, H. Matsunaga, T. Nakashima, K. Wada, A. Yamakata, O. Ishitani and K. Maeda, *J. Am. Chem. Soc.,* 2016, **138**, 5159.
23 J. J. Walsh, C. Jiang, J. Tang and A. J. Cowan, *Phys. Chem. Chem. Phys.,* 2016, **18**, 24825.
24 K. Wada, M. Eguchi, O. Ishitani and K. Maeda, *ChemSusChem*, 2017, **10**, 287.
25 G. Zhao, H. Pang, G. Liu, P. Li, H. Liu, H. Zhang, L. Shi and J. Ye, *Appl. Catal. B: Environ.*, 2017, **200**, 141.
26 M. F. Kuehnel, K. L. Orchard, K. E. Dalle and E. Reisner, *J. Am. Chem. Soc.*, 2017, **139**, 7217.
27 J. Lin, Z. Pan and X. Wang, *ACS Sustainable Chem. Eng.,* 2014, **2**, 353.
28 Y. Hori, H. Wakebe, T. Tsukamoto and O. Koga, *Electrochim. Acta*, 1994, **39**, 1833.
29 A. Yamakata, M. Yoshida, J. Kubota, M. Osawa and K. Domen, *J. Am. Chem. Soc.*, 2011, **133**, 11351.
30 A. Yamakata, T.-a. Ishibashi and H. Onishi, *J. Phys. Chem. B*, 2001, **105**, 7258.
31 K. Furuhashi, Q. Jia, A. Kudo and H. Onishi, *J. Phys. Chem. C*, 2013, **117**, 19101.
32 X. Li, G. Hartley, A. J. Ward, P. A. Young, A. F. Masters and T. Maschmeyer, *J. Phys. Chem. C* 2015, **119**, 14938.

33 B. Ravel and M. Newville, *J. Synchrotron Rad.,* 2005, **12**, 537.
34 H. Kato, K. Asakura and A. Kudo, *J. Am. Chem. Soc.,* 2003, **125**, 3082.
35 K. Maeda, K. Teramura, D. Lu, T. Takata, N. Saito, Y. Inoue and K. Domen, *J. Phys. Chem. B,* 2006, **110**, 13753.
36 K. Maeda, D. Lu, K. Teramura and K. Domen, *Energy Environ. Sci.,* 2010, **3**, 471.
37 K. Maeda, T. Ohno and K. Domen, *Chem. Sci.,* 2011, **2**, 1362.
38 K. Maeda, K. Ishimaki, M. Okazaki, T. Kanazawa, D. Lu, S. Nozawa, H. Kato and M. Kakihana, *ACS Appl. Mater. Interfaces,* 2017, **9**, 6114.
39 L. H. Tjeng, M. B. J. Meinders, J. van Elp, J. Ghijsen, G. A. Sawatzky and R. L. Johnson, *Phys. Rev. B*, 1990, **41**, 3190.
40 V. K. Kaushik, *J. Electron Spectroscopy and Related Phenomena*, 1991, **56**, 237.
41 K. Muraoka, H. Kumagai, M. Eguchi, O. Ishitani and K. Maeda, *Chem. Commun.,* 2016, **52**, 7886.
42 R. Godin, Y. Wang, M. A. Zwijnenburg, J. Tang and J. R. Durrant, *J. Am. Chem. Soc.*, 2017, **139**, 5216.
43 M. Xu, L. Han and S. Dong, *ACS Appl. Mater. Interfaces,* 2013, **5**, 12533.
44 S. Ma, J. Xue, Y. Zhou and Z. Zhang, *RSC Adv.,* 2015, **5**, 40000.
45 M. Wu, J.-M. Yan, X.-W. Zhang, M. Zhao and Q. Jiang, *J. Mater. Chem. A,* 2015, **3**, 15710.

TOC graphics
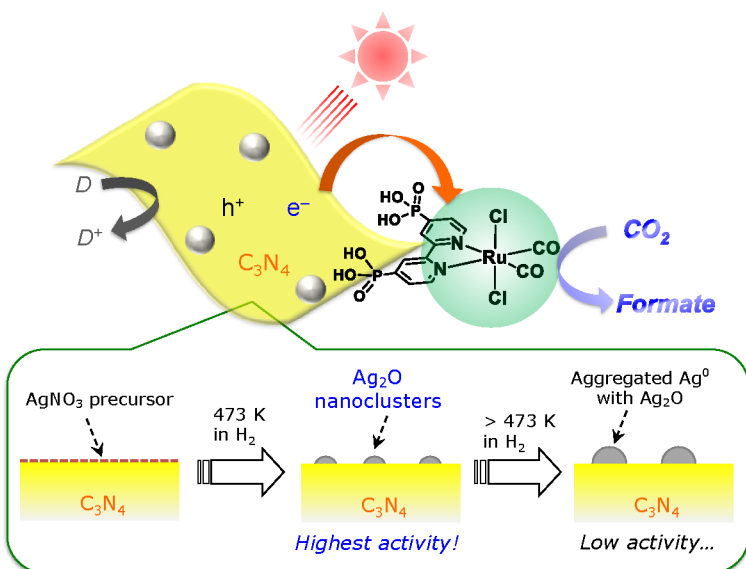
Text

Structure of Ag species that efficiently promote visible-light CO_2 reduction into formate by a Ru-complex/Ag/C_3N_4 hybrid photocatalyst was elucidated.